Received: 27 November 2019 | Revised: 18 March 2020 | Accepted: 4 April 2020

DOI: 10.1002/er.5462

SPECIAL ISSUE RESEARCH ARTICLE

INTERNATIONAL JOURNAL OF ENERGY RESEARCH WILEY

Computer modeling of electrochemical processing of waste nuclear fuel

Alexander Y. Galashev[1] | **Alexander I. Manzhurov**[1,2] | **Yuri P. Zaikov**[1,2]

[1]Institute of High-Temperature Electrochemistry, Ural Branch, Russian Academy of Sciences, Academic Str. 20, Yekaterinburg, Russia

[2]Ural Federal University named after the first President of Russia B.N. Yeltsin, Yekaterinburg, Russia

Correspondence
Alexander Y. Galashev, Institute of High-Temperature Electrochemistry, Ural Branch, Russian Academy of Sciences, Yekaterinburg 620990, Russia.
Email: galashev@ihte.uran.ru

Funding information
The State Atomic Energy Corporation ROSATOM, Grant/Award Number: The agreement No. 18, 04.06.2018

Summary

The purpose of the work is to study the influence of the electrodes geometry and the mutual arrangement of functional elements in the working space of a metallization electrolyzer on the distribution of the oxygen flux density in the electrolyte, as well as on the distribution of electric and temperature fields. In a computer model, the stationary operation mode of the electrolyzer for processing spent nuclear fuel immersed into the LiCl molten salt with the addition of Li_2O was studied. The calculations were performed using the ANSYS software package. We studied eight designs of the electrolyzer, which differ in the immersion depth of the anodes into the melt as well in the types anode protective covers and the cathode baskets. Verification based on the comparison of the computer modeling with experimental data indicates the adequacy of the models used. The electrolyte velocity field and the temperature field are calculated, as well as the steady-state picture of the distribution of electric current density over the working space of the electrolyzer. The efficiency of the electrochemical cell is determined.

KEYWORDS

current density, electrolyzer, model, spent nuclear fuel, uranium dioxide

1 | INTRODUCTION

World energy needs are largely met through nuclear power, which includes the creation of compact reactors.[1-3] Due to the fact that a huge amount of spent nuclear fuel (SNF) is accumulated in countries receiving and using nuclear energy, there is an urgent need for profitable nuclear energy generation and safe SNF reprocessing. In this regard, the electrochemical method of SNF reprocessing is an unparalleled option and it brings hope of creation of the closed nuclear fuel cycle.

Funding information: The agreement No. 18, 04.06.2018 under support of the State Atomic Energy Corporation ROSATOM. The work was carried out as a part of R&D Development of technology and equipment for the pyrochemical processing of SNF of fast neutron reactors" in the "Breakthrough" project area.

To date, significant laboratory studies have been performed on the reduction of SNF by the pyrochemical electrolytic method.[4-8] The amount of reduced U in all cases, as a rule, did not exceed 100 g. The method of electrochemical reduction of UO_2 in the molten LiCl salt with the addition of Li_2O requires accurate adherence to the process parameters. For example, the maximum allowable current density at the anode should not exceed 0.55 A/cm^2. The potential of the anode during shutdown is another important characteristic. It should remain in the range from 2.5 to 2.9 V relative to Li^+/Li^0, which corresponds to the potential evolution of oxygen. The anode potential exceeding 3.0-3.2 V signals the beginning of the joint evolution of oxygen and chlorine. In this case, electrolysis must be stopped.

A complete understanding of the electrolytic process that occurs during the reduction of UO_2 in the molten

LiCl salt with the addition of Li_2O has not been achieved yet. However, the main directions for the development of the theory of this process have been identified. In particular, experimental and computer based diffusion models demonstrate that oxygen diffusion in the solid phase (UO_2) is a limiting factor in the reduction process in the case of a small mass (~ 3 g) of SNF.[9] When developing a process theory, two circumstances must be taken into account. First, the initial stage of reduction is associated with the chemical reaction between Li and UO_2. Second, reduced SNF is gradually becoming electrically conductive, and at the final stage of reduction, the participation of lithium in this process is not needed. A purely electrochemical reduction occurs by transferring electrons to U^{4+} ions and releasing O^{2-} ions into the electrolyte. Papers[10,11] provide an assessment of the safety of SNF under conditions of permanent disposal. The simulation of the heat treatment of irradiated nuclear fuel and the emission of fission products was performed.[12] A theoretical study of changes in the structure and mechanical properties of reduced UO_2 at oxygen removal from this system was studied in Ref.[13] But there is practically no computational modeling aimed at upgrading the laboratory metallization electrolyzer used to recover UO_2.

In view of the high radiation hazard when handling SNF, it seems very important to imitate the process of processing of this hazardous material using the computer modeling. The advantage of this approach is not only its safety, but also the possibility of working out through a large number of modeling options to find the right way to solve the problem. Time factor is not less important here. Computer modeling can significantly (at times) speed up the study. Modeling using the ANSYS software package and using optimal design strategies can enrich both technological and electrochemical theories of a metallization electrolyzer functioning and provide some guidelines for the optimal design and operation of practical electrolysis systems designed to recover SNF. Using ANSYS, several aspects of UO_2 handling have been investigated. Among them were the following: thermal and mechanical properties of a fuel element of a thermal neutron reactor[14]; joint analysis of temperature distributions, oxygen diffusion, and deformation to predict the exact behavior of a nuclear fuel tablet (UO_2) during cracking[15]; accident analysis of heat sink loss in a spent fuel tank[16]; simulation of the thermal behavior of shipping containers, in particular, a container for SNF assembly.[17]

The specific goal of this study is to create an adequate model of an electrochemical device used to recover SNF (UO_2). This study should not only improve the existing laboratory facility, but also it should optimize the electrolytic process of metallic uranium separation. To achieve this, we investigated the influence of the geometry of the electrodes and the working space, as well as the mutual arrangement of the elements of the metallization electrolyzer, on the distribution of the density of oxygen flows as well as electric and temperature fields.

2 | EFFICIENCY CRITERION

To manufacture such complex electrochemical device as a metallization electrolyzer is both the knowledge of the composition and characteristics of materials suitable for long-term operation of the device and the possibility to choose correctly individual elements of different chemical nature, and chemical indifference during the operation are of great importance. Relevant information should be obtained by creating and optimizing the parameters of model prototypes of electrochemical devices. The electrolyzer should ensure high energy efficiency of the SNF recovery process, as well as the environmental safety of this process. A quantitative assessment of the choice of the optimal SNF recovery mode and the balanced geometry of the electrolyzer working space can be made by introducing such characteristics as the process efficiency. The electrical and chemical energy supporting the SNF reduction process does not completely transform into useful work. Energy in the electrolyzer is spent on the creation of fluid motion and chemical reactions. The energy spent on the metallization of the SNF loaded into the electrochemical device is considered to be the useful one. The inefficient part of the energy will be dissipated as heat. During the reprocessing ofSNF, several types of work including pressure, viscous forces, gravity, and kinetic energy creation are performed. In addition to viscous scattering, the heat of chemical reactions is present. If the total input power to control volume of the electrolyzer is $P = I \times \Phi$, then its efficiency can be determined as

$$\eta = \int_{V_e} \mathbf{u} \cdot \mathbf{F}_e / P,$$

where I is the total current, Φ is the potential difference between the positive and negative electrodes, and $\mathbf{u}$ and $\mathbf{F}_e$ are the vectors of the corresponding velocity and force.

Since the actions of all ineffective forces in the electrolyzer are extremely difficult to take into account, the efficiency of this unit can be taken as

$$\eta_1 = -G_{UO_2}(T) \cdot M_U / (\tau_U P_e), \quad (1)$$

where G_{UO_2} is the specific free energy of the formation of uranium dioxide, M_U is the mass of the obtained metallic

uranium, and τ_U is the time of formation of metallic uranium during electrolysis.

The temperature dependence of the quantity G_{UO_2} is reproduced in Figure 1 according to the data calculated by us using the HSC Chemistry (Outotec, Ver. 9.9) computer program. These data are in good agreement with the results reported in Ref[18] in the field of their determination ($298 \le T \le 673$ K). The obtained value $G_{UO_2} = -986.5$ kJ/kg at the temperature $T = 923$ K can be used to evaluate the efficiency of the laboratory electrolyzer for the electrolytic reduction of SNF according to the data given in Ref.[7] Substituting this value together with the data ($M_U = 15.86$ g, $\tau_U = 2.5 \cdot 3600$ s, $I = 4.2$ A, $\Phi = 3.2$ V) gives $\eta_1 = 0.13$.

Using formula (1) with a value of $\eta_1 = 0.13$ and performing the corresponding calculations, we determine the time $\tau_U = 11.6$ h required for the formation of metallic uranium with 100% yield at full UO_2 load of the cathode basket in the studied electrolytic cell models. This time is close to the corresponding time, observed in a real experimental electrolysis (it is available in the laboratory), which is usually 11-12 hours. This means that when loading 61 g of UO_2 into the basket (which is more than three times larger than the similar loading described in Ref.[7]), our laboratory electrolyzer has efficiency no worse than that of the laboratory electrolyzer presented in Ref.[7]

3 | GEOMETRIC MODEL OF THE ELECTROCHEMICAL CELL

In these calculation models, two anodes, which are shielded by high purity solid magnesium oxide covers,

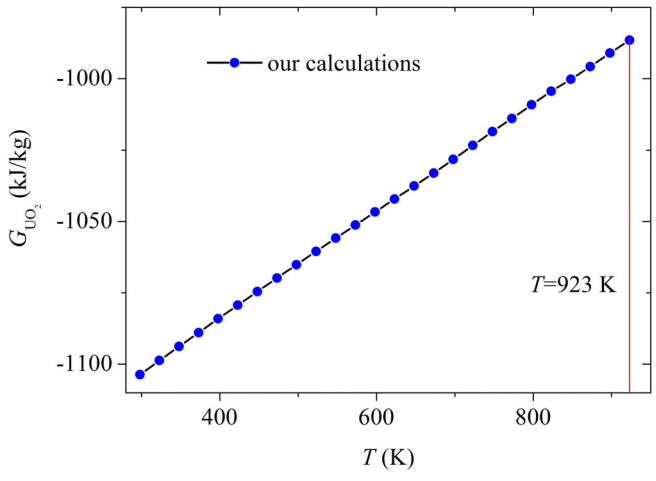

FIGURE 1 Calculated specific free energy of the formation of uranium dioxide obtained by us using the computer program HSC Chemistry. The UO_2 reduction temperature is $T = 923$ K [Colour figure can be viewed at wileyonlinelibrary.com]

are used. The variable parameters are the immersion depths of the anodes, protective covers and cathode baskets in the melt. The basic geometry of the cell is shown in Figure 2. A three-dimensional model of the cell (axonometric projection) without melt and SNF is shown in Figure 3.

The electrolyte container considered in the models is made of ceramic (MgO), wall thickness is 3 mm, height is 80 mm, diameter is 69 mm; the cathode basket is made of X18H10T stainless steel in the shape of a rectangular parallelepiped with dimensions of $40 \times 30 \times 7$ mm; a is the distance between the end face of the cathode basket and the bottom of the container (Figure 2). Dense ceramic nonconsumable anodes (composition of the NiO-Li_2O material) have the shape of a parallelepiped with dimensions of $6 \times 14 \times 45$ mm, the bevels along the edges of the faces are removed, and c is the distance from the end of the anode to the bottom of the container. Technological slots are made in the upper part of the anode, which is not immersed into the molten salt. A platinum wire with a diameter of 1 mm, which serves as the anode current lead, is wound through these slots. The cathode current lead, which has a rectangle form of 30×6 mm at the bottom, is made of molybdenum wire with a diameter of 1 mm. Ceramic covers for shielding anodes (100 mm long, 20 mm in diameter, with a wall thickness of 1.5 mm) are made of magnesium oxide; b is the distance from the end of the cover to the bottom of the container. A top view of the unloaded model of the electrolyzer is shown in Figure 3.

To calculate the effect of the immersion depth of the anodes, shielding covers, and the cathode basket on the temperature field and the distribution of electric current density in the cell volume, a, b, and c values were varied (Table 1).

ANSYS uses the finite element method (FEM) to simulate physical processes. The use of FEM suggests that the problem to be solved is formulated in the form of differential equations or in a variational formulation. The simulated object is divided into finite elements. As a result of such breakdown, a grid is created from the boundaries of the elements. Grid nodes can be supplemented by nodal points on the border and inside the elements. Using constants and options, finite elements are endowed with certain properties. In particular, this defines the material of the elements. At grid nodes, independent parameters or degrees of freedom are calculated. The system of equilibrium equations for the finite element model is compiled. Grid generation is the basis for representing and solving equations in matrix form.

Using several test calculations, the optimal grid resolution (870 000 nodes) was achieved. At the same time, it was taken into account that despite the fact that a larger

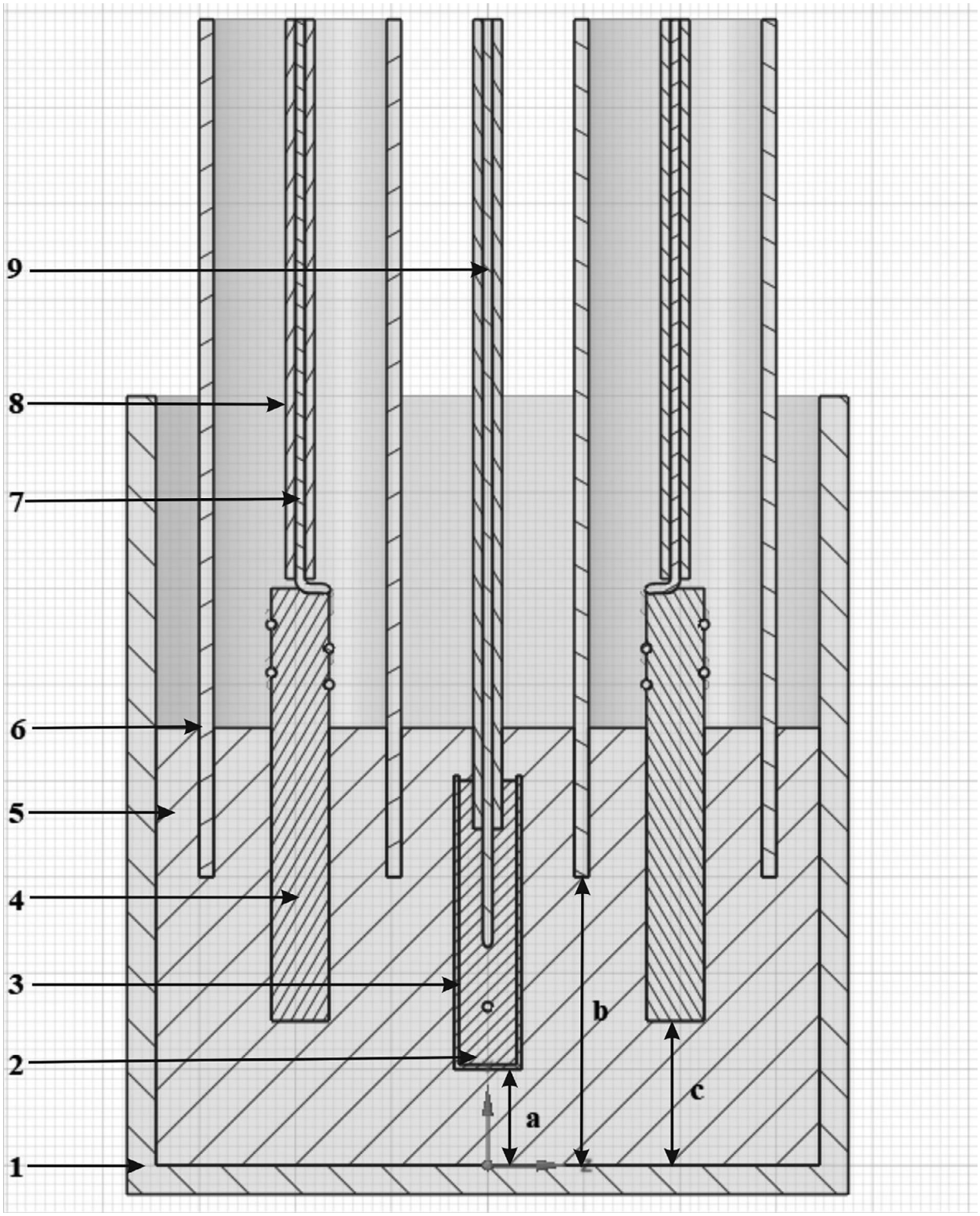

FIGURE 2 Vertical section of the cell: 1—container for electrolyte; 2—SNF location; 3—cathode basket; 4—ceramic nonconsumable anodes; 5—LiCl-Li_2O melt; 6—protective covers of anodes made of dense high purity MgO ceramics; 7—anode current leads; 8—ceramic straw made of MgO; 9—cathode current supply

number of nodes give a more accurate solution, excessive mesh refinement does not compensate the assumptions made in the model. With an accuracy of 1%-2%, independence of the results from the choice of mesh was achieved. The mesh smoothing procedure, which allows one to move nodes and control the number of iterations of the smoothing process, was used. Along with standard mechanical verification, a nonlinear verification of the

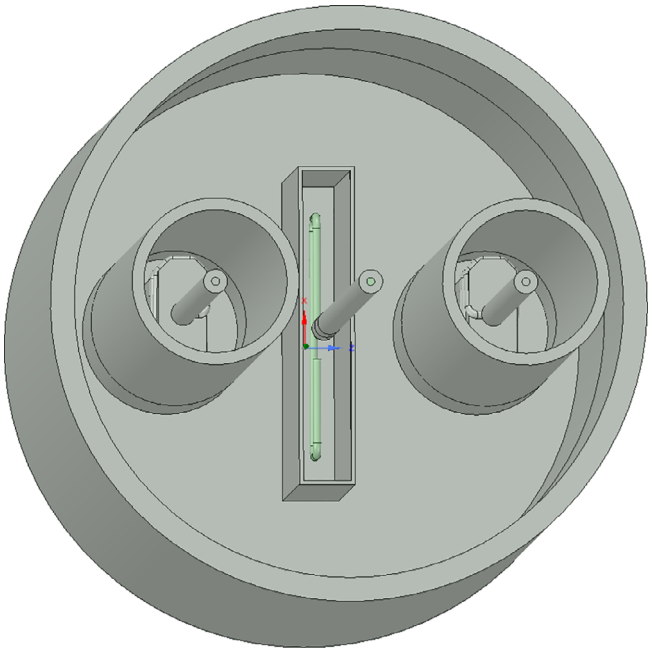

FIGURE 3 Three-dimensional model of a metallization electrolyzer without melt and SNF [Colour figure can be viewed at wileyonlinelibrary.com]

TABLE 1 Variation parameters of the immersion of the parts of the cell into the melt

Design number	*a* (mm)	*b* (mm)	*c* (mm)
1	10	30	15
2	10	15	15
3	10	25	10
4	10	10	10
5	5	30	15
6	5	15	15
7	5	25	10
8	5	10	10

shape of the elements was used to calculate the temperature fields in the case of hydrodynamic analysis. For objects of the same type, the element translation method was used, which allows one to create regular grids and to achieve better convergence of calculations. In energetically stressed sections of the system, the number of divisions forming a grid was increased. A mesh with the same density was generated on the contacting surfaces. To solve nonlinear problems, the control over convergence in forces, moments, displacements, and rotation is required. The parameters governing convergence were selected empirically. The results were verified by comparing them with experimental data observed in a laboratory electrochemical cell. In particular, good agreement was reached in the values of temperature and current density in the areas of electrolyzer of the greatest interest.

4 | PHYSICAL MODEL

We will consider the processes of convective flow of a heterogeneous mixture in the electrolyzer (near the anode in the presence of an electric field) in the approximation of a monodisperse mixture.[19,20] When describing hydrodynamic processes, the following equations and relationships were used.

The Navier-Stokes equations for the case of temperature dependence of the density of the medium[21]:

$$\rho_0\left(V_x\frac{\partial V_x}{\partial x}+V_y\frac{\partial V_x}{\partial y}+V_z\frac{\partial V_x}{\partial z}\right)=-\frac{\partial P}{\partial x}+\eta\left(\frac{\partial^2 V_x}{\partial x^2}+\frac{\partial^2 V_x}{\partial y^2}+\frac{\partial^2 V_x}{\partial z^2}\right)$$

$$\rho_0\left(V_x\frac{\partial V_y}{\partial x}+V_y\frac{\partial V_y}{\partial y}+V_z\frac{\partial V_y}{\partial z}\right)=-\frac{\partial P}{\partial y}+\eta\left(\frac{\partial^2 V_y}{\partial x^2}+\frac{\partial^2 V_y}{\partial y^2}+\frac{\partial^2 V_y}{\partial z^2}\right)$$

$$\rho_0\left(V_x\frac{\partial V_z}{\partial x}+V_y\frac{\partial V_z}{\partial y}+V_z\frac{\partial V_z}{\partial z}\right)=-\frac{\partial P}{\partial z}+\eta\left(\frac{\partial^2 V_z}{\partial x^2}+\frac{\partial^2 V_z}{\partial y^2}+\frac{\partial^2 V_z}{\partial z^2}\right)+\rho(1-\beta T),$$

where V_α is the component of the fluid velocity at the point (x, y, z); ρ_0 and ρ are the densities of the medium at temperatures T_0 and T, respectively; η is the viscosity coefficient; and β is the coefficient of thermal expansion.

Incompressibility equation is as follows:

$$\frac{\partial V_x}{\partial x}+\frac{\partial V_y}{\partial y}+\frac{\partial V_z}{\partial z}=0.$$

The heat equation, which takes into account the volumetric heat source associated with the decay of SNF and Joule heat,[17] is as follows:

$$V_x\frac{\partial T}{\partial x}+V_y\frac{\partial T}{\partial y}+V_z\frac{\partial T}{\partial z}=\chi\left(\frac{\partial^2 T}{\partial x^2}+\frac{\partial^2 T}{\partial y^2}+\frac{\partial^2 T}{\partial z^2}\right)+\frac{Q_{\mathrm{SNF}}}{\rho c}+\frac{J^2}{\sigma\rho c},$$

where χ is the thermal diffusivity, Q_{SNF} is the power of the volumetric heat source associated with the decay of SNF, c is the specific heat, ρ is the density, J is the current density, and σ is the specific conductivity.

Stefan-Boltzmann law for a real body is presented below:

$$S = \varepsilon c_0 T^4,$$

where S is the energy luminosity, $c_0 = 5.67032 \cdot 10^{-8}$ W/m^2/K^4 is the Stefan - Boltzmann constant. The values of the coefficient ε are determined by the nature of the body, the state of its surface, and temperature.

The first law of Kirchhoff (the law of conservation of electric charge)[22] is as follows:

$$\frac{\partial J_x}{\partial x} + \frac{\partial J_y}{\partial y} + \frac{\partial J_z}{\partial z} = 0, \quad (2)$$

where J_α is the corresponding component of the current density.

Maxwell's equation (rot $\mathbf{E} = 0$) and Ohm's law are provided below:

$$\frac{\partial E_z}{\partial y} - \frac{\partial E_y}{\partial z} = 0, \frac{\partial E_x}{\partial z} - \frac{\partial E_z}{\partial x} = 0, \frac{\partial E_x}{\partial y} - \frac{\partial E_y}{\partial x} = 0 \quad (3)$$

$$J_x = \sigma E_x, J_y = \sigma E_y, J_z = \sigma E_z, \quad (4)$$

where $E_{\boldsymbol{\alpha}}$ is the α-component of the electric field strength.

The mass of the substance formed on the electrode can be calculated using the first Faraday law of electrolysis:

$$m = \left(\frac{It}{F}\right)\left(\frac{M}{z}\right), \quad (5)$$

where m is the mass of the substance formed on the electrode, $F = 403.965$ kJ/mol is the Faraday constant, M is the molar mass of the substance, z is the number of electrons in the reaction, t is the electrolysis time, and I is the electrolysis current.

The reaction of oxygen formation at the anode has the form:

$$2O^{2-} - 4e^- = O_2.$$

The specific mass flux of the formed oxygen per unit time can be calculated according to Equation (5). The molar mass of oxygen is $M = 32 \cdot 10\text{-}3$ kg/mol, $z = 4$. Therefore, it is equal to

$$q_m = 8.2914 \cdot 10^{-8} \left[\frac{\text{kg}}{\text{s} \cdot \text{A}}\right] \cdot J \left[\frac{\text{A}}{\text{m}^2}\right].$$

The ANSYS software package assumes the function of defining and implementing boundary conditions. To do this, it is sufficient to create a geometric model of the problem and introduce the minimum number of parameters associated with the boundary and initial conditions. In this package, many solution details are hidden from the user. Hiding routine operations greatly facilitates the study. The following boundary conditions are most often used.

Since the walls of the electrolyzer and its structural elements are impermeable, and the LiCl-Li_2O melt has a viscosity $\eta(T)$, the usual boundary condition for the velocity is as follows:

$$v_n = 0, v_\tau = 0,$$

where v_n and v_τ are the normal and tangent velocity components, respectively.

Modeling of flow in a porous medium, which represents SNF (UO_2) in the model, is a special case. It was assumed that on the permeable walls of the basket the condition is true

$$v_n = v_b,$$

where v_b is the average flow rate of the electrolyte in the cell.

If the walls of the electrolyzer consist of sections of ideal conductors ($\sigma = \infty$) and insulators ($\sigma = 0$), then the boundary conditions for the flow region are

$$E\tau = 0, \text{for } \sigma = \infty$$

where $E\tau$ is the tangential component of the electric field strength

$$J_n = 0, \text{при } \sigma = 0,$$

where J_n is the normal component of the current density.

Using the experimentally established fact that the porous SNF medium is completely saturated with electrolyte, we made simplifications, assuming that the electrical conductivity of this medium is fully consistent with the electrical conductivity of the electrolyte.

The following parameters were used for calculations: external heating temperature from the furnace side $T_1 = 650°$C; ambient temperature $T_2 = 20°$C; heat generation associated with radioactive decay of SNF $Q_{SNF} = 9860$ W/m^3; coefficient of convective heat transfer of the parts of the cell with the environment $\alpha = 1.0$ W/m^2·K.

The properties of the materials used in the calculation (density, electrical conductivity, thermal conductivity, heat capacity, body emissivity, etc.) were set depending on the temperature.[23-26]

The conductivity of the LiCl-Li_2O melt in the model was calculated taking into account the influence of the presence of oxygen using the expression[19,20]:

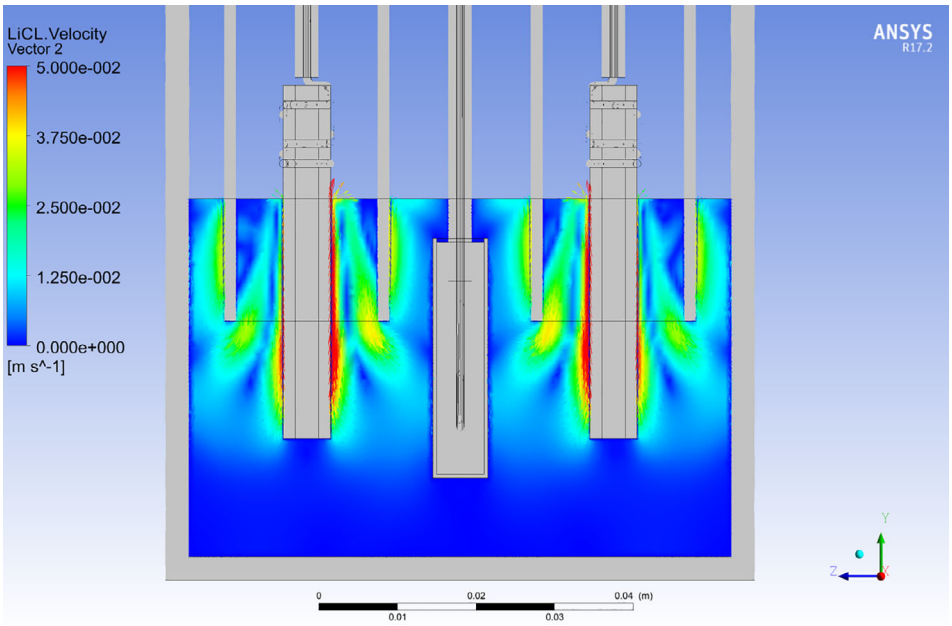

FIGURE 4 Field of melt velocities; main vertical slice for design No. 1 [Colour figure can be viewed at wileyonlinelibrary.com]

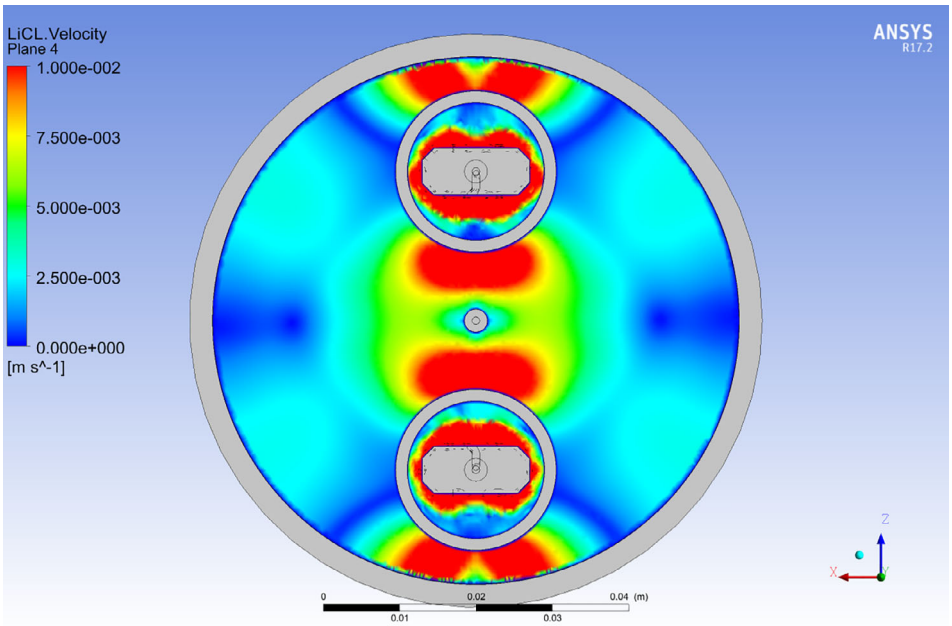

FIGURE 5 Field of melt velocities; horizontal section near the surface of the melt for design No. 1 [Colour figure can be viewed at wileyonlinelibrary.com]

$$\sigma_{\mathrm{LiCl-Li_2O}}(T) = \frac{\sigma_{\mathrm{LiCl}}(T)}{0.22\cdot\exp\left(4.22\cdot O_2^{\mathrm{VF}}\right) + 3.53\cdot10^{-6}\cdot\exp\left(17.06\cdot O_2^{\mathrm{VF}}\right) + 0.78},$$

where $\sigma_{\mathrm{LiCl}}(T)$ is the electrical conductivity of the pure LiCl melt depending on temperature and O_2^{VF} is the volume fraction of oxygen in the melt.

5 | RESULTS

In general, the melt velocities are low near the cathode basket of design No. 1 (as well as near the baskets of other designs) due to the deceleration of the melt meeting this obstacle (Figure 4). Melt velocities are maximum near the surfaces of the anodes, especially those facing the cathode. However, on the opposite side in the lower part of the anodes, the melt velocities near the surfaces of these electrodes are high too. Such speeds appear due to the surface turbulence associated with the intensive vertical movement of oxygen bubbles formed on the anode.

Figure 5 shows the distribution of electrolyte velocities near the surface of the melt for design No. 1. It can be seen that the maximum surface velocities of the melt are achieved in areas directly adjacent to the anodes and from two sides of the outer shells surrounding them. In

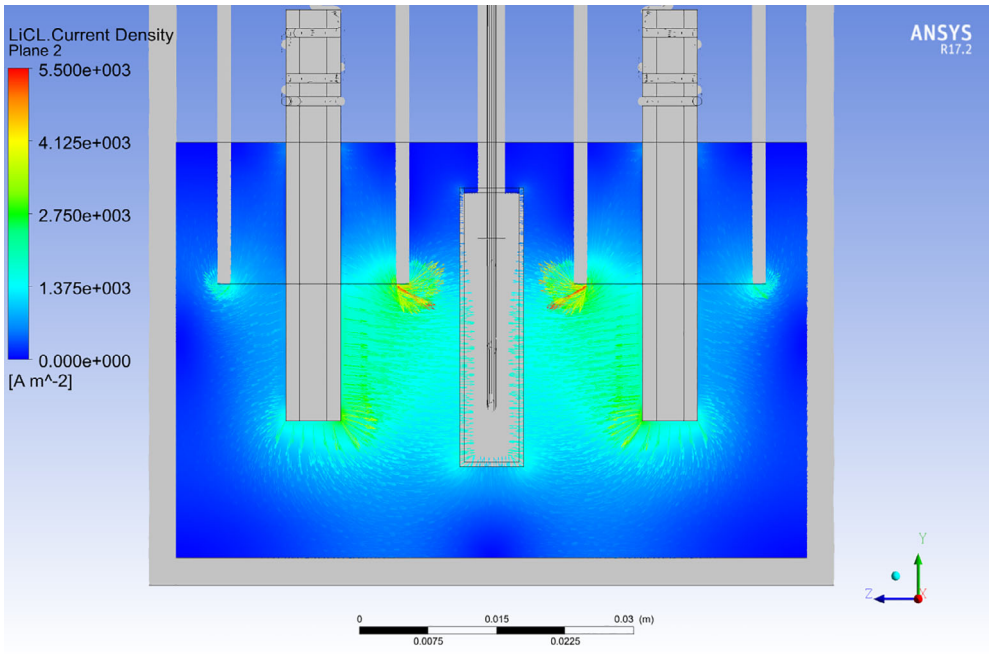

FIGURE 6 Distribution of current densities in the melt; main vertical slice for design No. 1 [Colour figure can be viewed at wileyonlinelibrary.com]

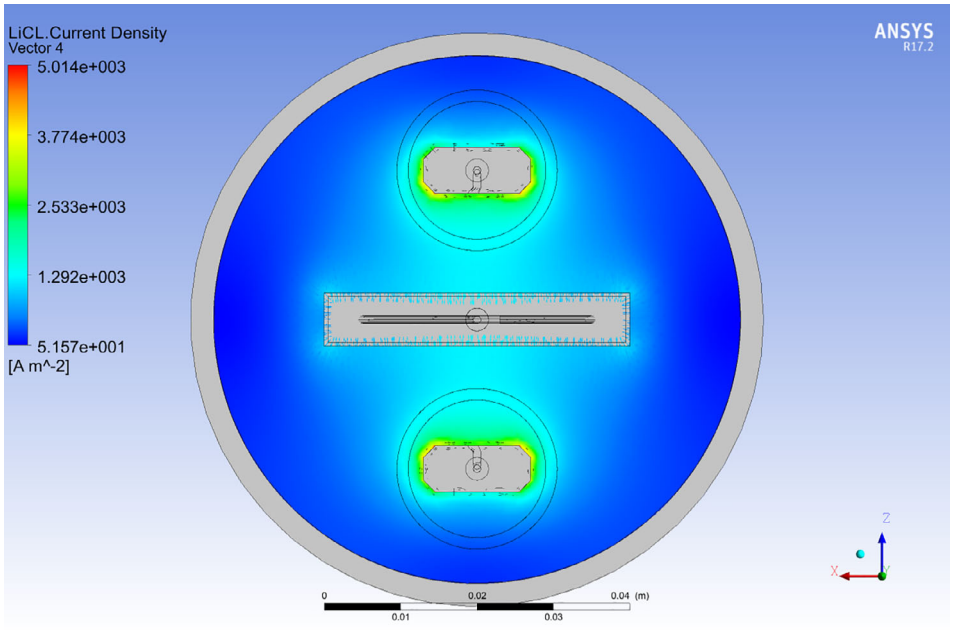

FIGURE 7 Distribution of current densities in the melt; horizontal section at the ends of the anodes for design No. 1 [Colour figure can be viewed at wileyonlinelibrary.com]

both cases, the high velocity of the electrolyte is associated with the rise and release of oxygen. The oxygen velocity field in the system is much similar to the electrolyte velocity distributions shown in Figures 4 and 5 (See Data S1). This means that the flow of oxygen in the electrolyte is crucial to the hydrodynamics of the entire electrolyte.

When constructing the distribution of the current density in the melt, the maximum permissible value of 0.55 A/cm^2 was taken for the upper boundary J (Figure 6). On the main vertical slice of structure No. 1, the critical value of the current density is not exceeded. An increased current density is observed in the lower parts of the electrodes and casings, as well as in the space between the bottoms of the anodes and casings corresponding to each other.

A horizontal slice made at the ends of the anodes also indicates the absence of a critical current density in this area of construction No. 1 (Figure 7). An even lower current density is observed near the bottom of the cathode basket.

The viscosity of the melt helps to reduce the velocity of the melt near the walls of the electrochemical cell. Figure 8 shows that this in turn creates a higher

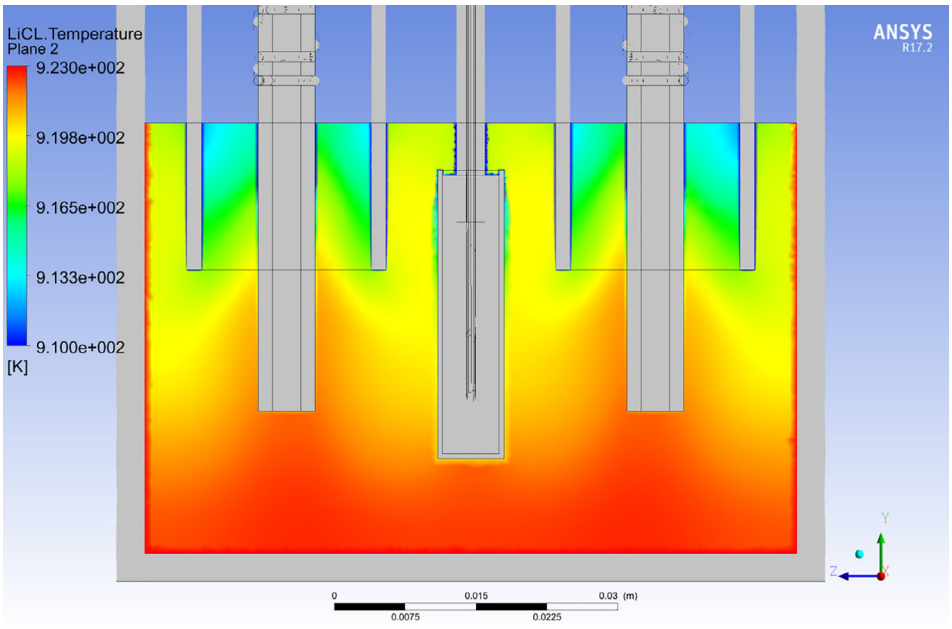

FIGURE 8 Temperature distribution in the melt in the main vertical section for model No. 1 [Colour figure can be viewed at wileyonlinelibrary.com]

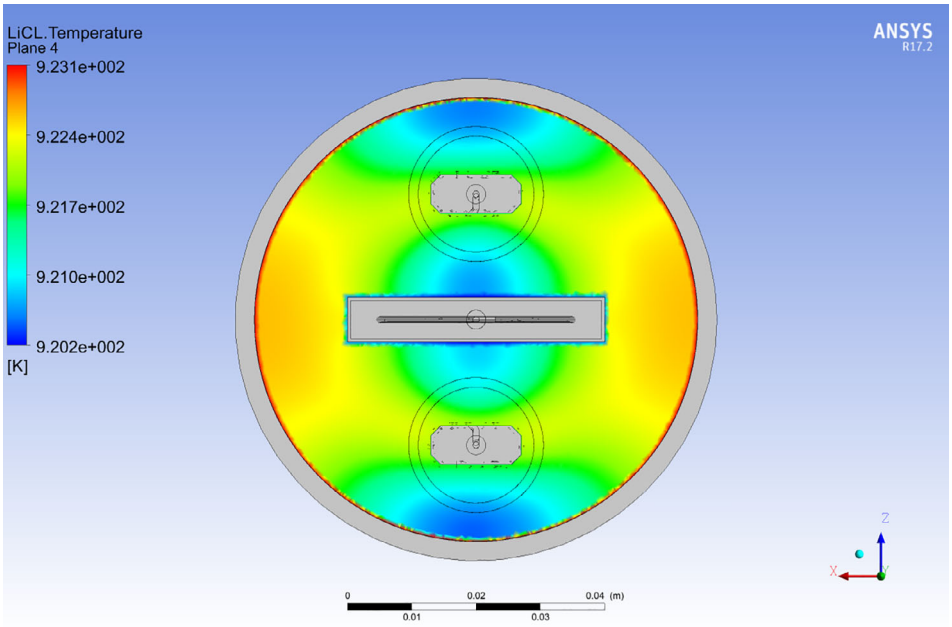

FIGURE 9 Temperature distribution in the melt in the horizontal section at the ends of the anodes for model No. 1 [Colour figure can be viewed at wileyonlinelibrary.com]

temperature near the walls of the container. In addition, the region of low melt velocities that does not contribute to the temperature equalization falls on the lower part of the container space (below the bottom of the cathode basket). It is the region, where the temperatures exceeding the temperature on the melt surface by 10°C-20°C, are observed. Due to the presence of a certain cooling of the melt from the side of solid structural elements (current leads, anodes, and covers) directly or through other elements communicating with the atmosphere, the temperature of the electrolyte in the upper part of the container decreases.

Figure 9 shows that in the melt a slight temperature change in the horizontal section of the electrochemical cell at the level of the ends of the anodes is observed. The temperature differences in different parts of the electrolyte at this level can reach 3 K. The regions with lower temperature are located in the central region of the cathode basket as well as in the regions opposite the wide side of the anodes situated not far from the walls of the electrochemical cell. Higher temperatures are held in the areas between the narrow faces of the cathode basket and the container walls opposite them. The highest temperature (923 K) belongs to a very thin layer directly adjacent to the walls of the container.

The configurations of the anodes No. 1, 3, 5, and 7 (partially open anodes) are more suitable for experiments with a ceramic crucible for melt, due to the lack of interaction between oxygen and ceramics. The maximum values of current density and temperature obtained in all eight designs of the electrolyzer are shown in Table 2.

During the electrolysis process, special attention should be paid to the value of current density at the anodes, since at the values of 0.55 A/cm^2 and higher, the process of chlorine evolution together with oxygen can begin on the anode. This reaction leads to the chlorination of the components of the electrode, change in its composition and loss of electrical conductivity. The obtained results and the above-described conditions for the current density measurements made it possible to compare all models and to choose the most optimal design of the metallization electrolyzer. As a result, under the same boundary conditions, only models No. 1, and three fully comply with the requirements for the cell. It is also possible to use model No. 5, however, there is a danger of local excess of current density limit values. The maximum values of the temperature in the electrolyte are quite close in all considered designs of the electrolyzer.

Figure 10 illustrates that, the temperature distribution in the solid components of the electrochemical cell is characterized by a sharp contrast between the temperature of the elements outside the cell body and the temperature of the solid components present inside the cell, including the steel container of the cell. These temperatures may differ more than two times. However, the cathode basket with UO_2 placed in the electrolyte is fully supported at the given temperature (923 K).

TABLE 2 Maximum current densities near the anode and maximum temperatures of the molten salt at different anode immersion depths, anode covers and cathode baskets

Design number	J_{max}, A/sm^2	T_{max}, °C
1	0.5014	651.039
2	1.5300	653.690
3	0.4977	652.888
4	1.3070	652.945
5	0.5562	652.562
6	1.6750	654.847
7	0.8479	652.508
8	2.2080	654.897

6 | DISCUSSION

Under the same boundary conditions, eight different models of the electrolyzer were tested. It turned out that only models No. 1, and 3 completely satisfy the conditions for successful electrolysis. It is risky to use anodes with geometry No. 5 due to the local excess of current density values at their ends. For all other options, a significant excess of permissible current density values was recorded. First of all, this applies to the models, in which the anodes are completely covered by casings. In these cases, the anodes have very small working areas.

Laboratory tests of cathode baskets showed that the completeness of SNF reduction depends on their shape and size, as well as on the location of the anodes relative to the basket. The geometric dimensions are dictated by

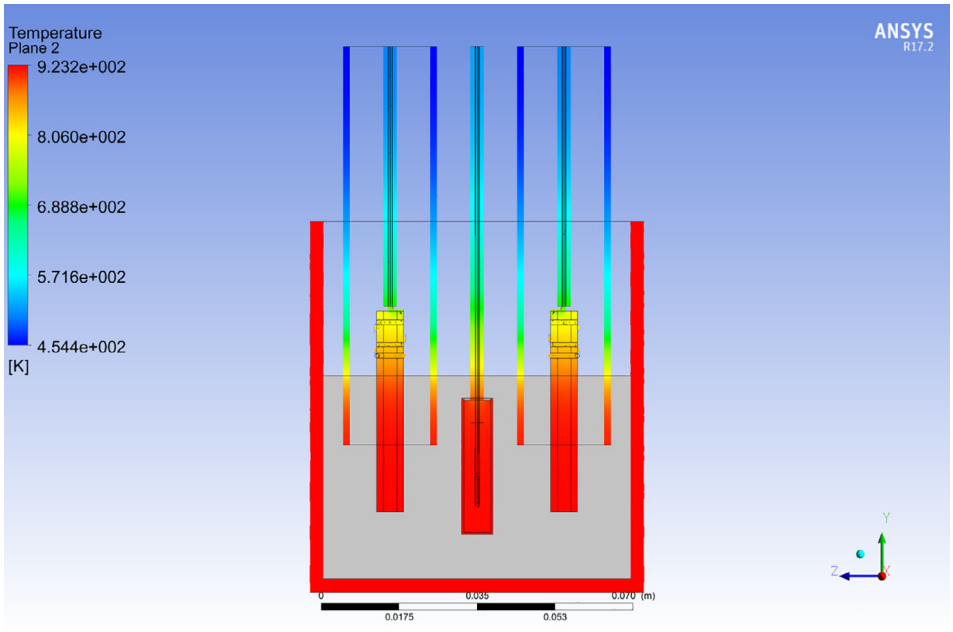

FIGURE 10 Temperature distribution in the main vertical section of the solid components of the electrochemical cell for design No. 1 [Colour figure can be viewed at wileyonlinelibrary.com]

the parameters of the electrolytic reduction process. It was shown that an increase in the thickness of the porous medium encountered by the electrolyte on the way from the anode to the cathode by over 12-15 mm, as a rule, leads to the incomplete reduction of UO_2 even when the amount of transmitted electric charge is twice as large as the theoretical value which is necessary for a complete recovery. In the present work, the test with the loaded UO_2 cathode basket was performed taking into account this fact. We varied only by the location of the electrodes relative to the container, as well as their relative position. It turned out that such manipulations allow identifying the optimal configuration of the electrolyzer, in which chlorine cannot be released on the anode together with oxygen. The calculated distributions of current density and temperature in the electrolyte indicate the absence of any obstacles for 100% recovery of SNF.

The passage of ions through a porous medium was studied in Ref.[27] We first consider the delay in ionic conductivity during the current passage of the loaded UO_2 cathode basket. The electrical conductivity of a porous medium impregnated with an electrolyte depends on the ratio of the mass of the solid to the mass of the electrolyte contained in it and, especially, on the conditions of impregnation. As a rule, a very low electrical conductivity of a porous medium immersed into the electrolyte is observed until the porosity of the medium reaches ~18%.[27] This result can be interpreted in the following form: the impregnation of the porous medium with electrolyte begins when the porosity reaches ~18%. Exceeding the threshold value of conductivity leads to an exponential growth of the latter.

First of all, the electrolyte penetrates into the pores due to capillary forces. The electrolyte occupying the external pores makes the main contribution to the electrical conductivity of the porous material. At the same time, internal nanopores retain the electrolyte inside, preventing it from escaping from the porous material. Moreover, the fraction of delayed electrolyte due to loss of a continuous path for ions in a porous medium can reach 50%. In fact, the effect of reducing the electrical conductivity of the fuel basket is significantly enhanced by chemical reactions leading to the formation of Li_2O, as well as the release of this unstable compound from the porous medium into the electrolyte.

Thus, the SNF basket is a serious obstacle to the passage of ions. Hydraulic resistance inhibits the penetration of electrolyte into the porous UO_2 medium, as a result of which the inequality $C^* > C^0$ can be achieved, where C * and C^0 are the current and initial ion concentrations near the walls of the porous material, respectively. In this case, a reverse current may occur, which reduces the concentration of C*[28]

$$J = -C^* \cdot F \cdot \sqrt{\frac{D\pi}{t}}, \quad (6)$$

where J, D, and F are the current density, ion diffusion coefficient, and the Faraday number, respectively. This current decreases in time as $1/\sqrt{t}$. Together with the ions coming from the volume of the electrolytic cell, it helps to collect ions near the side walls of the cathode basket where a very high current density appears. This leads to a significant local heating of the above region.

The ions present in the electrolyte are carriers of an electric charge, and the movement of these ions creates an electric current. For model No. 1, the current density in the electrolyte near the open parts of the anodes is higher than near the cathode basket. This is due to the more intense movement of the electrolyte in the vicinity of the anodes due to the formation and rise of oxygen bubbles in this region. Therefore, if there is a process of electrolytic reduction of SNF, then the cathodic and anodic regions are the most problematic places to maintain this process. It must be ensured that clogging does not occur in the cathode region when ions move through a porous medium (SNF). It is also necessary that in the anode region the current density does not exceed the critical value of 0.55 A/cm^2.

7 | CONCLUSION

This paper presents the results of computer simulations of various operating electrolytic cells used in the reduction of UO_2 to uranium metal. The calculations were performed using the ANSYS CFX program. The results were verified by comparison with experimental data observed in a laboratory electrochemical cell. The influence of the geometric features of the design of the electrolyzer (eight different variations in the immersion depth of the anodes, baskets and protective covers in the molten electrolyte) on the processes occurring in it was studied. Among the various options, a modified (improved) electrochemical cell, that is, an electrolyzer with anodes protected by shells, was considered. The use of anodes completely covered by covers is advisable in cases, when the crucible is made of nickel, because it allows one to remove almost all the gas released through the space between the anode and the cover, thereby eliminating the interaction of oxygen with the material of the container, resulting in an undesirable nickel oxide formation. Electrolysis with partially open anodes is recommended to be carried out in a ceramic container, since the generated oxygen is distributed throughout the entire volume of the electrolyte. Near

the side surface of the cathode basket, a high current density may appear. This occurs when the thickness of the porous SNF layer, which separates the cathode and electrolyte, begins to exceed the value determined for the given design of the electrolyzer. The reason for this lies in the increase in the electrical resistance of the layer associated with an increase in the layer thickness due to the appearance of tortuosity, and, possibly, blockage of the channels along which ions move.

The main findings of the work are as follows:

1 A computer model of the electrolyzer was created, the main operating characteristics of which (melt velocity field, temperature field in the melt and in solid elements of the electrochemical device, and current density distribution) correspond to the characteristics of a laboratory electrolyzer used to recover SNF.
2 The structural elements of the anode, which have a strong influence on the field of melt velocities as well as on the distribution of temperature and current density over the volume of the electrolytic cell, are revealed.
3 The use of anode shielding covers were found to increase the current density in the lower part of the cathode basket and to decrease the average melt velocity near the surface of the anodes. It was possible to ensure that the bulk of oxygen (up to 90%) goes into the space bounded by the walls of the anode covers.
4 The calculated characteristics of the main parameters of a functioning electrolyzer allow a deeper understanding of the process of UO_2 reduction in the model and, on this basis, allow improving the design of the corresponding laboratory unit as well as allow optimizing the process of electrolytic reduction of SNF.

ACKNOWLEDGEMENTS

The present paper is partly supported by the agreement No. 18, 04.06.2018 under support of the State Atomic Energy Corporation ROSATOM. The work was carried out as a part of R&D "Development of technology and equipment for the pyrochemical processing of SNF of fast neutron reactors" in the "Breakthrough" project area.

SUPPORTING INFORMATION

Additional supporting information may be found online in the Supporting Information section at the end of this article.

ORCID

Alexander Y. Galashev https://orcid.org/0000-0002-2705-1946

REFERENCES

1. Nguyen T, Choe J, Ebiwonjumi B, Lemaire M, Lee D. Core design of long-cycle small modular lead-cooled fast reactor. *Int J Energy Res*. 2019;43:254-273.
2. Wang X, Zhuang K, He X, Seidl M, Macian-Juan R. Neutron physics of the liquid-fuel heat-pipe reactor concept with molten salt fuel–static calculations. *Int J Energy Res*. 2019;43:7852-7865.
3. Dai Z, Wang C, Zhang D, Tian W, Qiu S, Su G. Thermoelectric characteristics analysis of thermionic space nuclear power reactor. *Int J Energy Res*. 2020;44:855-868.
4. Choi E-Y, Kim J-K, Im H-S, et al. Effect of the UO_2 form on the electrochemical reduction rate in a LiCl–Li_2O molten salt. *J Nucl Mater*. 2013;437:178-187.
5. Hur J-M, Hong S-S, Lee H. Electrochemical reduction of UO_2 to U in a LiCl–KCl-Li_2O molten salt. *J Radioanal Nucl Chem*. 2013;295:851-854.
6. Sakamura Y, Kurata M, Inoue T. Electrochemical reduction of UO_2 in molten $CaCl_2$ or LiCl. *J Electrochem Soc*. 2006;153(3): D31-D39.
7. Choi E-Y, Won CY, Cha J-S, et al. Electrochemical reduction of UO_2 in LiCl–Li_2O molten salt using porous and nonporous anode shrouds. *J Nucl Mater*. 2014;444:261-269.
8. Choi F-Y, Jeong SM. Electrochemical processing of spent nuclear fuels: an overview of oxide reduction in pyroprocessing technology. *Prog Nat Sci: Mater Int*. 2015;25(6):572-582.
9. Yao B, Cheng Z, Xiao Y, Jia Y, Lin R, He H. Diffusion-based kinetic model for the electroreduction of UO_2 in LiCl-Li_2O melt. *J Electrochem Soc*. 2019;166(15):D826-D833.
10. Zhu Z. The Electrochemical Study of Simulated Spent Nuclear Fuel (SIMFUEL) Corrosion Under Permanent Disposal Conditions [Electronic thesis and dissertation repository]. 5787; https://ir.lib.uwo.ca/etd/5787; 2018.
11. Metz V, Geckeis H, Gonzalez-Robles E, Loida A, Bube C, Kienzler B. Radionuclide behaviour in the near-field of a geological repository for spent nuclear fuel. *Radiochim Acta*. 2012; 100:699-713.
12. Shcherbina NS, Kivel N, InesGünther-Leopold I. Effect of redox conditions on the fission products release from irradiated oxide fuel. *Procedia Chem*. 2012;7:104-109.
13. Galashev AY, Ivanichkina KA, Zaikov YP. Computational study of physical properties of low oxygen UO_{2-x} compounds. *J Solid State Chem*. 2020;286:121278.
14. Pandey KM, Sarkar A. Structural analysis of nuclear fuel element with ANSYS software. *Int J Eng Technol*. 2011;3(2):187-192.
15. Otercus S, Madenci E. Peridynamic modeling of fuel pellet cracking. *Eng Fract Mech*. 2017;176(15):23-37.
16. Grazevicius A, Kaliatka A. Modelling of the spent fuel heat-up in the spent fuel pools using one-dimensional system codes and CFD codes. *Kerntechnik*. 2017;82(3):316-333.
17. Gokselkinav AD, Ayhan H, Ergun S. Thermal analysis of spent nuclear fuel shipping cask. Paper presented at: Annual International Conference NUCLEAR POWER FOR THE PEOPLE, At Bulgaria; 2013; Vol 18: 1-12. 15 September, 2013.
18. Pescatore C. *Free Energy of Formation of U_3O_7 in the Temperature Range 25 to 400°C. BNL53I72/UC-70*. Upton, NY: Brookhaven National Laboratory; 1988:1-7.
19. Nigmatulin RI. *The Dynamics of the Multiphase Media (in Russian). Part 1*. Moscow, Russia: Nauka; 1987.

20. Nigmatulin RI. *Fundamentals of Mechanics of Heterogeneous Media (in Russian)*. Moscow, Russia: Nauka; 1978.
21. Landau LD, Lifshitz EM. *Fluid Mechanics*. Course of Theoretical Physics. Vol 6. 2nd ed. Oxford, UK; New York, Beijing, China; Frankfurt, Germany; Sao Paolo, Brazil; Sydney, Australia; Tokyo, Japan; Toronto, Canada: Pergamon press; 1987.
22. Landau LD, Lifshitz EM. *Electrodynamics of Continuous Media*. A Course of Theoretical Physics. Vol 8. Oxford, UK: Pergamon Press; 1960.
23. Bates JL, Hinman CA, Kawada T. Electrical conductivity of uranium dioxide. *J Am Ceram Soc*. 2015;50(12):652-656.
24. Salema AM, Mokhtarb M, El-Shobaky GA. Electrical properties of pure and Li_2O-doped NiO/MgO system. *Solid State Ion*. 2004;170:33-42.
25. Van Artsdalen ER, Yaffe IS. Electrical conductance and density of molten salt systems: KCl–LiCl, KCl–NaCl and KCl–KI. *J Phys Chem*. 2015;59(2):118-127.
26. Bobkov VP, Fokin LR, Petrov EE, Popov VV, Rumiantsev VN, Savvatimsky AI. *Thermophysical Properties of Materials for Nuclear Engineering: A Tutorial and Collection of Data*. Vienna, Austria: IAEA; 2008.
27. Mizuhata M, Kitamura M, Deki S. Nano-pore effect on ionic conduction of non-aqueous $LiClO_4$ solution coexisting with porous solid materials. *Electrochemistry*. 2003;71(12):1093-1095.
28. Gelloz B, Bsiesy A, Gaspard F, Muller F. Conduction in porous silicon contacted by a liquid phase. *Thin Solid Films*. 1996;276:175-178.

SUPPORTING INFORMATION

Additional supporting information may be found online in the Supporting Information section at the end of this article.

How to cite this article: Galashev AY, Manzhurov AI, Zaikov YP. Computer modeling of electrochemical processing of waste nuclear fuel. *Int J Energy Res*. 2020;1–13. https://doi.org/10.1002/er.5462